JOURNAL OF MECHANICAL ENGINEERING AND SCIENCES
ISSN: 2289-4659 e-ISSN: 2231-8380
VOLUME 19, ISSUE 4, 2025, 10953 - 10965
DOI: https://doi.org/10.15282/jmes.19.4.2025.9.0857

RESEARCH ARTICLE

CFD analysis of the impact of building shapes on the performance of wind-driven natural ventilation

Kalyan Kumar Das[1], Rupam Deka[2]*, Partha Protim Borthakur[2], Chinmoy Jit Sarma[3], Piyush Singh[1]

[1] Department of Mechanical Engineering, Assam Engineering College, Guwahati 781013, Assam, India
[2] Department of Mechanical Engineering, Dibrugarh University, Dibrugarh 786004, Assam, India
[3] Assam Energy Institute, Sivasagar, A Centre of Rajiv Gandhi Institute of Petroleum Technology, Sivasagar 785663, Assam, India

ABSTRACT - The widespread use of natural ventilation in buildings is limited despite its numerous benefits, mainly due to the challenges associated with enhancing ventilation performance. This study employs numerical simulations to examine the influence of building shapes on ventilation performance in naturally ventilated building models. The wind-driven cross-ventilation through buildings with flat and pitched-roofs was investigated. Various building configurations were considered based on the position of openings in the building façades. To assess the natural ventilation efficiency of these configurations, numerical calculations were carried out to evaluate the normalised average velocity magnitude (V*), velocity homogeneity index (H), and air change rate (ACH). The results showed that a configuration with a windward opening near the ground and a leeward opening near the roof yielded the highest V* and H values for both flat and pitched-roof buildings. However, for the same configuration, V* and H were 17.69% and 13.24% higher in flat-roof buildings than in pitched-roof buildings. The highest ACH value in both flat-roof and pitched-roof buildings was obtained for the configuration with a windward opening at the mid-height of the building façade and a leeward opening near the ground. The ACH value for this configuration was 2.8% higher in flat-roof buildings than in pitched-roof buildings. These findings can support the design and optimisation of natural ventilation systems in buildings with improved ventilation performance.

ARTICLE HISTORY
Received : 22nd Jan. 2025
Revised : 05th June 2025
Accepted : 26th Oct. 2025
Published : 29th Dec. 2025

KEYWORDS
Natural ventilation
Cross-ventilation
Computational fluid dynamics
Ventilation performance
Indoor air quality
Building aerodynamics

1. INTRODUCTION

The recent outbreak of the COVID-19 pandemic has once again brought attention to the extensive use of natural ventilation in residential and commercial buildings, schools, and hospitals. In natural ventilation, the exchange between outdoor fresh air and indoor air takes place continuously, resulting in dilution of the indoor contaminants. It was found that compared to a confined space, the infection rate by the SARS-CoV-2 was reduced significantly in a naturally ventilated space [1]. Hence, spreading diseases like COVID-19 can be controlled in naturally ventilated buildings. Using natural ventilation in buildings also helps the occupants reduce occurrences of other diseases like Sick Building Syndrome (SBS).

The energy consumption in buildings constitutes a significant portion of global energy use, emphasizing the need for enhanced energy efficiency measures in building design and operation. Over the years, this has become a focal area of research with natural ventilation emerging as an attractive solution due to its inherent energy efficiency [2]. Natural ventilation leverages environmental airflows to exchange indoor and outdoor air, reducing the reliance on mechanical ventilation systems. Researchers and designers have long been interested in its potential, with various strategies being employed to optimise its effectiveness. Typically, natural ventilation is facilitated through strategically placed openings, such as windows and doors, on building façades. Two primary types of natural ventilation are widely recognised: single-sided ventilation and cross-ventilation. In single-sided ventilation, air exchange occurs through openings on a single façade, limiting its effectiveness due to constrained airflow paths. Conversely, cross-ventilation involves openings on opposing façades, enabling air to flow across the building. This mechanism significantly enhances ventilation efficiency, making cross-ventilation the preferred choice among engineers and architects [3].

The performance of natural ventilation systems is primarily assessed based on two critical criteria: indoor air distribution (IAD) and indoor air quality (IAQ). Quantitative evaluation of IAD often involves parameters like normalised average velocity magnitude (V*) and velocity homogeneity index (H), both of which indicate the uniformity and effectiveness of airflow within a space. Higher values of these parameters signify improved mixing and distribution of air. Additionally, qualitative assessments of IAD can be conducted using velocity contours and vector plots that visually represent airflow patterns. IAQ, on the other hand, is measured using the air change rate (ACH) and the mean age of air (MAA). ACH quantifies the rate at which indoor air is replaced with outdoor air, reflecting the overall ventilation rate, while MAA provides a quantitative measure of air residence time within an indoor space, which is indicative of ventilation performance and indoor air quality [4].

***CORRESPONDING AUTHOR | Rupam Deka** | ✉rupamdeka@dibru.ac.in

Previous research highlights the importance of these metrics in evaluating ventilation performance. For instance, Zhou *et al.* [5] employed MAA, while Bayoumi [6] utilized both MAA and ACH to assess the efficacy of natural ventilation. Sacht and Lukiantchuki [7] analysed ACH and airflow direction, establishing a link between air exchange rates and ventilation effectiveness. The use of ventilation rates as a benchmark for performance evaluation is widespread [8-10], with Hwang and Gorlé [11] incorporating MAA to provide a more comprehensive assessment. Similarly, Díaz-Calderón *et al.* [12] applied a combination of V*, H, and normalised volume flow rate to evaluate natural ventilation, reflecting the multi-dimensional approach to assess performance. The effectiveness of cross-ventilation is significantly influenced by various building features, including the position, size, and shape of openings as well as the geometry of the building itself. Among these, the location of openings plays a pivotal role. Cross-ventilation configurations can be classified as symmetric, where openings are axially aligned, or asymmetric, where openings are diagonally positioned. While most existing studies focus on symmetric configurations [13, 14], the exploration of asymmetric configurations has been relatively limited. To address this gap, several researchers [15, 16] have investigated the impact of both symmetric and asymmetric configurations on cross-ventilation performance. Tominaga and Blocken [17] demonstrated that airflow rates are strongly influenced by the position of the windward opening, with higher rates observed when the windward opening is placed at the top, regardless of the leeward opening's position. Moey *et al.* [18] corroborated these findings, noting that symmetric configurations with both openings at the top achieve superior ventilation rates compared to asymmetric setups. These observations align with earlier studies [19], reinforcing the critical role of opening placement in optimizing cross-ventilation systems.

The studies reviewed above predominantly focus on simple cubic buildings with flat-roofs, leaving a gap in understanding how building shapes influence natural ventilation performance. Building shapes play a critical role in determining pressure distribution around the structure, which directly impacts airflow and ventilation effectiveness [20]. This underscores the need to investigate natural ventilation in buildings with diverse geometric configurations to expand the scope of current research beyond basic cubic forms. Perén *et al.* [21] explored natural ventilation in buildings with sawtooth roofs featuring asymmetric openings. Their findings indicated that variations in the height of the leeward opening had minimal impact on the volume flow rate. Furthermore, negligible differences in the average velocity within the occupied space were observed when the leeward opening was located near the roof. This suggests that factors other than opening height may play a more significant role in influencing ventilation performance in such configurations. Similarly, Xing *et al.* [22] examined pitched-roof buildings with varying opening arrangements, finding that the positions of openings significantly affected internal pressure. This is a crucial consideration, as internal pressure impacts not only ventilation performance but also the structural integrity of the building, especially under varying wind conditions. Hayati *et al.* [23] compared airflow rates in buildings designed for cross-ventilation versus those with single openings. Their study revealed that cross-ventilation achieved substantially higher airflow rates. Moreover, the incident direction of the wind relative to the openings was critical; when the wind direction was perpendicular to the openings, airflow rates were significantly enhanced compared to parallel wind directions. These findings highlight the importance of wind direction in optimizing natural ventilation systems. Despite these advancements, there remains a lack of consensus on which building shapes and configurations yield the best natural ventilation performance. This ambiguity is particularly evident when comparing common building geometries, such as flat and pitched-roofs. Addressing this gap, the present study aims to comprehensively evaluate natural ventilation performance in buildings with flat and pitched-roofs, as these are among the most widely utilized shapes. The investigation considers multiple opening configurations to determine how the placement of openings on the building façades and building shapes collectively influence ventilation effectiveness.

The primary objective of this research is to identify the building geometry and an appropriate opening configuration for the given building geometry for which maximum natural ventilation performance is achieved. By focusing on parameters such as airflow distribution and rate of air exchange, this study seeks to provide actionable insights for architects and engineers. These insights not only enhance indoor air quality and occupants' thermal comfort but also promote energy-efficient building designs by leveraging passive ventilation strategies.

2. MATERIALS AND METHODS

To comprehensively analyse cross-ventilation flow in various building configurations, this study employs advanced computational techniques. Specifically, the three-dimensional steady-state Reynolds-averaged Navier–Stokes (RANS) equations are solved numerically to simulate airflow patterns and assess ventilation performance. The simulations are performed using the ANSYS Fluent software, version 19.0, a robust computational fluid dynamics (CFD) tool widely recognised for its accuracy and reliability in modelling complex fluid flows.

2.1 Building Configurations and Computational Domain

In the present investigation, two building models with flat and pitched-roofs (a roof pitch of 5:10) are considered. The length (l) and width (w) of both models are taken as 12 m and 6 m, respectively. In the case of the pitched-roof building models, the eave height (h) is fixed as 6 m, which is equivalent to the height of a two-storey building. However, to keep the internal volume of both models equal, a height of 6.75 m (h) is chosen for the flat-roof building models. Both building models consist of two openings of equal sizes, 6.0 m × 1.2 m (width × height), and are located on two opposite façades, i.e., windward and leeward façades. The schematic diagram of the building models is shown in Figure 1.

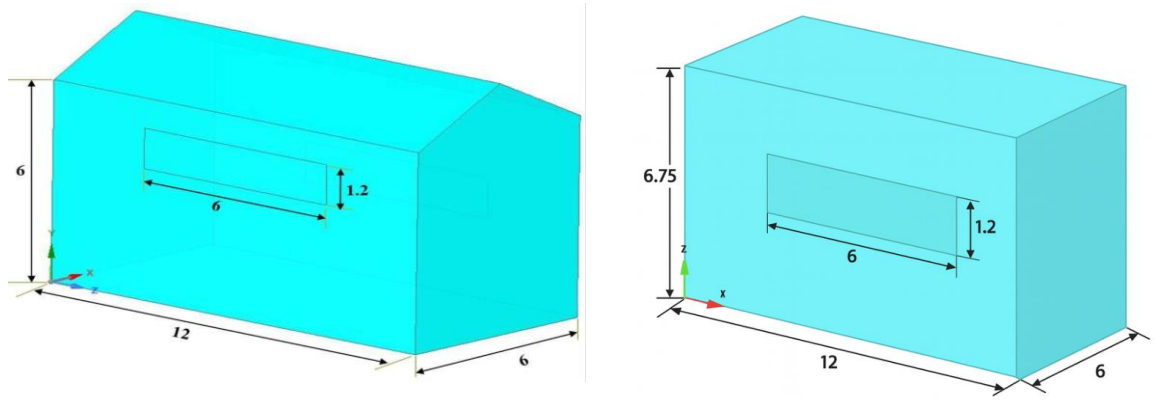

(a) (b)

Figure 1. Perspective view of the building models with dimensions (in metres) (a) pitched-roof and (b) flat-roof

The current study examines seven different opening configurations to evaluate the performance of natural ventilation in building models with flat and pitched-roofs. These configurations consist of two openings on the buildings' windward and leeward façades. The openings are located at different heights above the ground. The height of the centreline of the windward and leeward openings from the ground is indicated by L1 and L2 in Figure 2. Among these seven configurations, one has axial openings, i.e., the symmetric configuration (S-0), and in the rest of the configurations (A-1 to A-6), openings are located diagonally, i.e., asymmetric configurations. The details of these configurations are provided in Table 1.

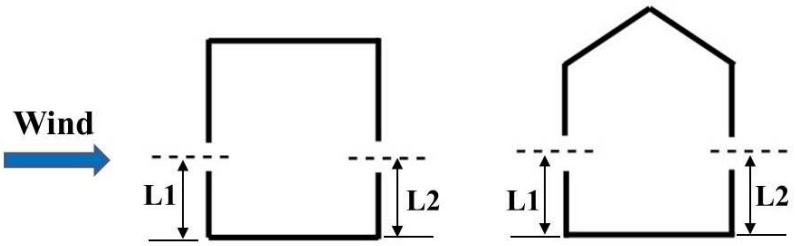

Figure 2. Schematic representation of a configuration with its openings located at the height of L1 and L2 from the ground

Table 1. Details of the configurations studied

Configurations	Height of the windward opening from the ground in metres (L1)	Height of the leeward opening from the ground in metres (L2)
S-0	3	3
A-1	4.5	3
A-2	4.5	1.5
A-3	3	4.5
A-4	3	1.5
A-5	1.5	4.5
A-6	1.5	3

To perform the numerical simulations, the computational domain was generated, and its dimensions are specified in line with prescribed best practice guidelines. The best practice guidelines were established in accordance with the recommendations of Franke *et al.* [24] and Tominaga *et al.* [25]. Moreover, Blocken *et al.* [26] suggested keeping the upstream length equal to three times the building height (i.e., 3*h*). A schematic diagram of the computational domain with its dimensions is shown in Figure 3. Further, to accomplish the numerical simulations, the computational domain is divided into a finite number of grids. The grids near the building are of the tetrahedron type; however, hexahedral elements and prism layers are employed far from the building model and near the solid boundary. Moreover, finer grids are used in the vicinity of the building (Figure 4).

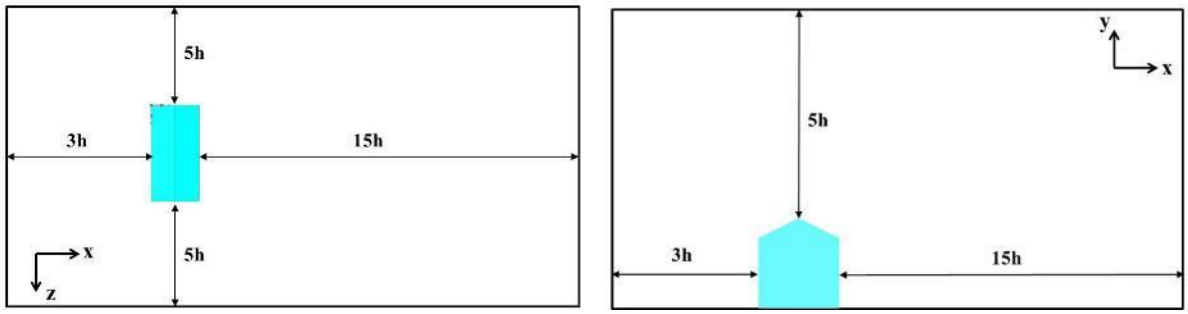

(a) (b)

Figure 3. Schematic diagram of the computational domain with its dimensions (a) top view (plan), (b) front view (elevation)

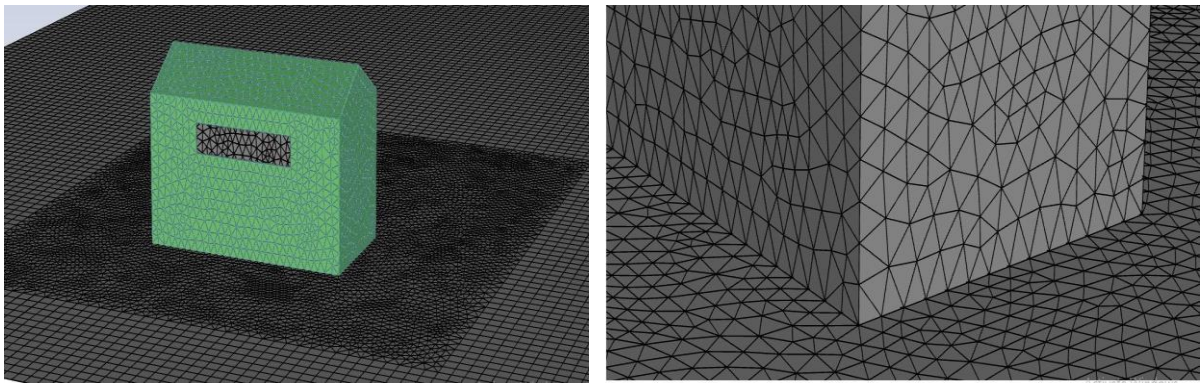

Figure 4. Perspective view of the grids generated on the computational domain

2.2 Boundary Conditions

The computational domain and its various boundaries are shown in Figure 5, and different boundary conditions employed for the solution of the governing equations are presented in Table 2.

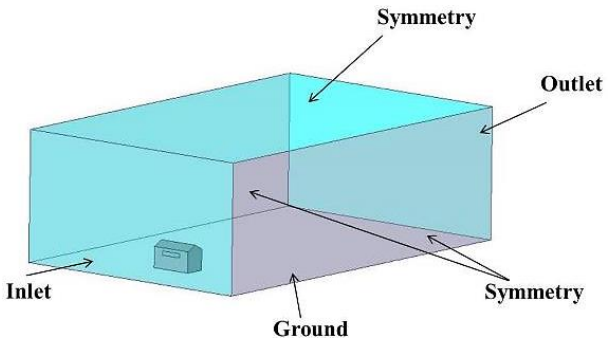

Figure 5. Schematic diagram of the computational domain with its various boundaries

Table 2. Details of the various boundary conditions employed in the present study

Name of the Boundary	Boundary Type	Boundary Settings
Inlet	Velocity Inlet	Logarithmic wind speed profile
Outlet	Pressure outlet	Atmospheric outlet
Lateral and Top Planes	Symmetry	The gradient of the variables is zero
Ground	Wall	No-slip condition with roughness
Building Façades	Wall	No-slip with smooth surface
Openings	Interior	–

The distributions of streamwise velocity profile U(y), turbulent kinetic energy k(y), turbulent dissipation rate (ε), and the specific dissipation rate (ω) at the inlet are provided below.

$$U(y) = \frac{u^*_{ABL}}{\kappa} \ln\left(\frac{y + y_o}{y_o}\right) \quad (1)$$

In Eq. (1), u^*_{ABL} is the friction velocity; y_o (= 0.0001 m) is the aerodynamic roughness length, y is the height coordinate, and κ is the von Kármán constant, which is taken as 0.4. The value of u^*_{ABL} is estimated as 0.347 m/s, considering the value of U as 10 m/s (=U_{ref}) at a height (y_{ref}=*h*=6 m) [27].

$$k(y) = a\left(I_u(y).u(y)\right)^2 \tag{2}$$

The constant a value in Eq. (2) was selected as 1 as recommended by Tominaga *et al.* [25]. The streamwise turbulent intensity ($I_u(y)$) profile obtained by [28] from the wind tunnel measurements is employed here, and the profile is defined in Eq. (3).

$$I_u(y) = \frac{1}{\ln\left(\frac{y}{y_o}\right)} \tag{3}$$

$$\varepsilon(y) = \frac{u^{*3}_{ABL}}{\kappa(y+y_o)} \tag{4}$$

$$\omega(y) = \frac{\varepsilon(y)}{C_\mu k(y)} \tag{5}$$

here, the value of the empirical constant, Cμ, is 0.09.

The building surfaces have a roughness constant (C_s) of 0.5 and a sand grain roughness height (k_s) of 0. For the ground surfaces, the value of C_s is assumed to be 1, and k_s is evaluated based on the values C_s and y_o according to Eq. (6).

$$k_s = \frac{9.793 y_o}{C_s} \tag{6}$$

2.3 Solver Settings

The current study utilised the ANSYS-FLUENT (v.2019) software package to numerically simulate the natural ventilation in buildings induced by the atmospheric wind. The governing equations, namely the three-dimensional steady-state Reynolds-averaged Navier-Stokes (RANS) equations, were solved using the k-ω Shear Stress Transport (SST) turbulence model, chosen for its effectiveness in capturing the complex flow dynamics around building structures. Detailed steps of the solution methodology adopted are presented in Table 3. Convergence criteria were rigorously defined to ensure accuracy in the numerical results. Specifically, convergence was considered achieved when the scaled residuals for continuity and the x, y, and z momentum, as well as the turbulent kinetic energy (k), reached a threshold value of 10^{-5} and 10^{-4} for specific dissipation rate (ω), respectively. Initial simulations exhibited oscillatory convergence, a common challenge in such complex CFD analyses. To address this, first, simulations were carried out for 5000 iterations before sampling and averaging the solutions over the final 500 iterations. A similar methodology has been applied in prior studies, as reported in [29].

Table 3. Summary of the solver settings used for numerical simulations

Turbulence Model	k–ω SST turbulence model
CFD code	ANSYS FLUENT 19.2
Algorithm	SIMPLE
Pressure Interpolation Scheme	Second-order
Discretization Scheme for Transport Equations	Second-order upwind scheme

2.4 Validation of the Numerical Simulations

A validation study was performed to assess the accuracy of the numerical model in predicting the cross-ventilation flow. The numerical model was validated against the experimental work of Karava *et al.* [19], who used a reduced-scale building model with a length and width of 0.1 m and a height of 0.08 m. The Reynolds number for the flow, based on an upstream wind speed of 6.97 m/s at the building height, was calculated to be 7.6×10^4. According to Cui *et al.* [30], the critical Reynolds number for indoor flow in wind-driven cross-ventilation is 15000. Given that the flow Reynolds number significantly exceeds this critical value, the flow is Reynolds-number independent, and therefore, the numerical solution is independent of model dimensions. Furthermore, Ramponi and Blocken [29] also endeavoured to replicate the wind tunnel measurement results obtained by [19]. The findings of the current numerical simulations exhibit a reasonably good agreement with both the above-mentioned studies (Figure 6(a)). Nevertheless, minimal discrepancies between the numerical and experimental results are noted. The inherent limitations of PIV measurements cause these minor aberrations. A schematic diagram of the model used for the validation study is shown in Figure 6(b).

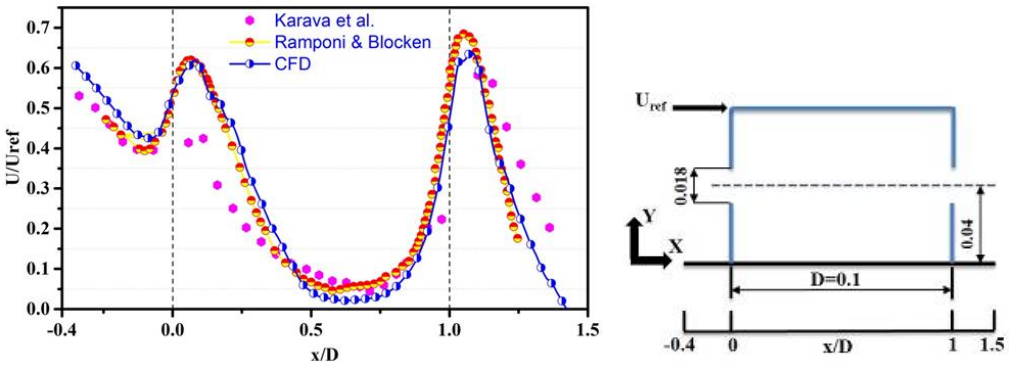

(a) (b)

Figure 6. (a) Comparison of U/Uref along the normalised streamwise direction (x/D), (b) Cross-sectional view of the building model used in the validation study

2.5 Grid Independent Test

To check that the simulation results are independent of the number of grids generated throughout the computational domain, a grid independence test was carried out for the configuration S-0 for a pitched-roof building model. Numerical simulations were performed on the said model using different types of grids as provided in Table 4, keeping all other conditions unchanged. The variation in normalised streamwise velocity (U/Uref) along the line joining the midpoints of windward and leeward openings is presented in Figure 7(a). The streamwise velocity distribution for basic and fine grids have shown negligible variation between them; however, for coarse grids, the difference is significant. Hence, further simulations were done using the basic grid to optimise the computational cost involved.

Table 4. Different types of grids

Type of grid	No. of elements
Coarse Grid	1721133
Basic Grid	2638635
Fine Grid	4193546

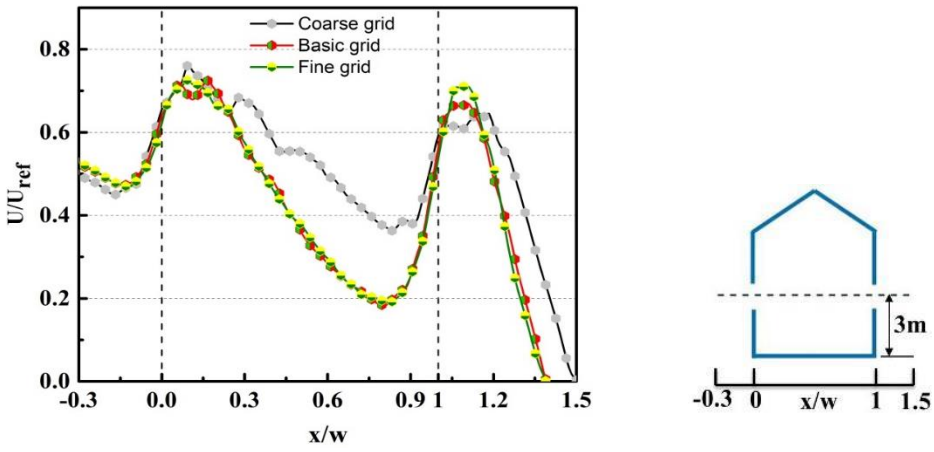

(a) (b)

Figure 7. (a) Comparison of U/Uref along the normalised streamwise direction (x / w) for different types of grids, (b) Cross-sectional view of the building model used in the grid-independent study

3. RESULTS AND DISCUSSION

This section presents the results of the current work, focusing on airflow patterns within the building models. To evaluate the ventilation performance of the various building configurations, parameters such as normalised average velocity magnitude (V*), velocity homogeneity index (H), and air change rate (ACH) are analysed and discussed.

3.1 Velocity Field

To better understand the airflow through the interior of the building models, velocity vector plots along the vertical mid-plane of the various configurations with flat and pitched-roofs are presented in Figures 8 and 9. The configurations considered in this study exhibit a similar airflow pattern for both roof shapes. The outdoor flow field is characterised by forming a standing vortex upstream of the building when the windward opening is located at or above mid-height of the windward wall. It is observed that the vortex size is larger when the windward opening is positioned above the mid-height

of the building. In contrast, the standing vortex is not observed when the windward opening is located below the mid-height of the windward wall. The distinctive feature of the indoor flow is marked by the formation of a jet as the air enters the building through the windward opening, progresses through the interior, and ultimately leaves through the leeward opening. The position of the windward opening governs the jet's trajectory. Regardless of the position of the leeward opening, the jet moves downwards when the windward opening is situated at mid-height or below the mid-height of the building wall. Conversely, the jet moves upwards when the windward opening is situated above the mid-height of the building wall. Furthermore, for configuration A-4 in both roof shapes, a continuous stream tube forms, connecting the windward and leeward openings; therefore, the flow experiences less resistance compared to other configurations. Moreover, for configurations with the windward opening located at mid-height, the jet moves downwards and a recirculation region is observed below the jet.

3.2 Normalised Average Velocity Magnitude (V*)

The normalised average velocity magnitude (V*) is determined using Eq. (7), as defined by [12]. The magnitude of V* is an indicator of indoor air distribution (IAD), and a higher value of V* signifies improved indoor air quality (IAQ).

$$V^* = \frac{V_{avg}}{U_{ref}} \tag{7}$$

here, V_{avg} and U_{ref} represent the average velocity magnitude in the indoor space and the reference velocity at the building height, respectively.

Figure 10(a) shows that in flat-roof buildings, the normalised average velocity magnitude (V*) in asymmetric opening configurations is higher than in symmetric configurations except for configuration A-4. The peak value of V* is attained for configuration A-5, in which the windward and leeward openings are located diagonally below and above the mid-height of the building façades, respectively. The increased magnitude of V* signifies enhanced indoor air quality in asymmetric opening configurations, resulting in improved natural ventilation effectiveness. The magnitude of V* in configuration A-5 is 45.45% higher than the symmetric configuration (S-0). In contrast, the magnitude of V* in configuration A-4 was found to be 8.5% lower than that of configuration S-0.

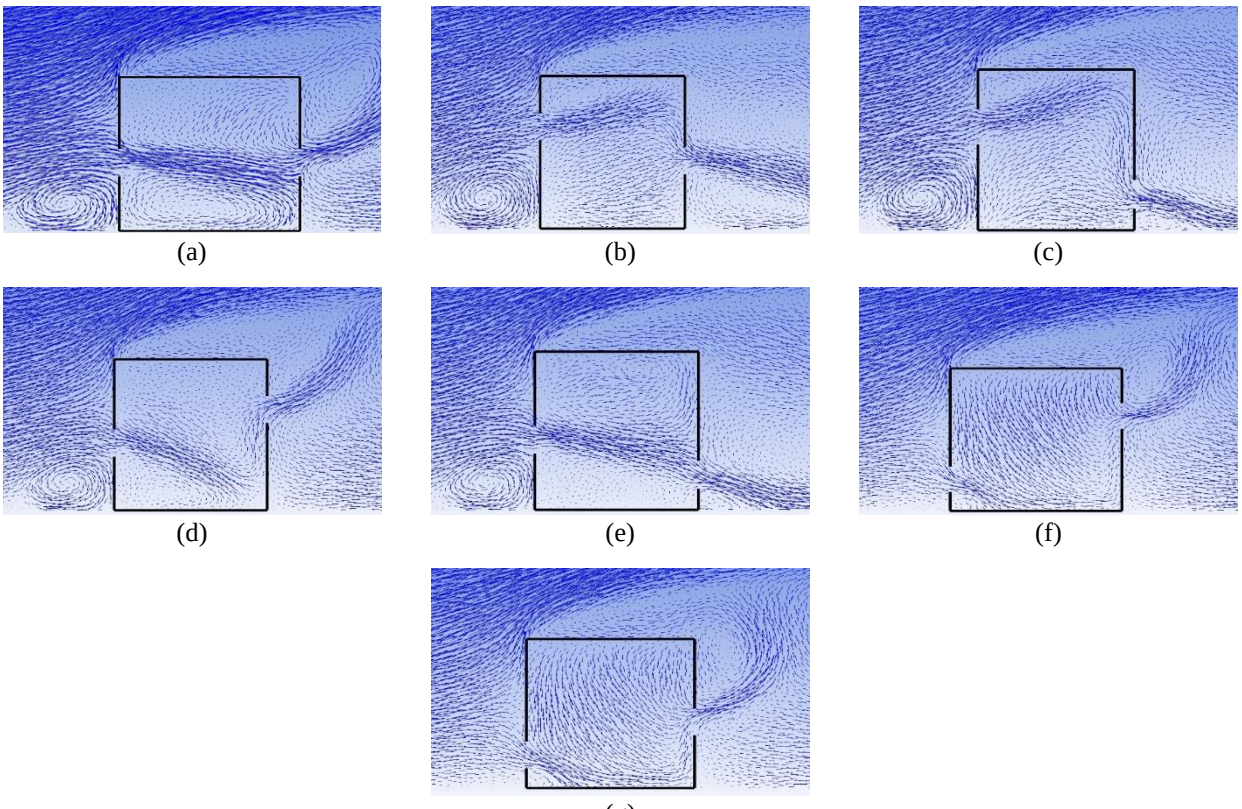

Figure 8. Velocity vector plot on the vertical mid-plane of a flat-roof building for configurations (a) S-0, (b) A-1, (c) A-2, (d) A-3, (e) A-4, (f) A-5, (g) A-6

Figure 10(b) compares the magnitude of V* between symmetric and asymmetric opening configurations in pitched-roof buildings. For all the asymmetric opening configurations, the magnitude of V* is found to be higher than the symmetric configurations. Further, the difference in magnitude of V* between configuration A-4, where the opening in the windward wall is situated at the mid-height, and the opening in the leeward side is located below the mid-height of the building wall, and S-0 (symmetric configuration) is less significant. Similar to the flat-roof buildings, the peak value

of V* is attained for the configuration A-5 in pitched-roof buildings, which is 31.48% higher than the symmetric configuration (S-0).

The variation in the magnitude of V* across different configurations can be attributed to the indoor airflow patterns specific to each configuration, as illustrated in Figures 8 and 9. The continuous 'stream tube' formed by the indoor air between the windward and leeward openings in configuration A-4 is responsible for the lower V* values observed for both roof shapes. Additionally, the air stream traverses a longer path in asymmetric configurations compared to symmetric ones as it moves from the windward to the leeward opening, leading to higher V* values in asymmetric configurations.

Notably, among the asymmetric opening configurations, A-5 exhibits the highest V* value, irrespective of building geometry. This is because the airstream must travel the longest path from the inlet to the outlet in A-5, as the airstream's radius of curvature is the largest in this configuration compared to other asymmetric configurations. Furthermore, Figure 11 demonstrates that the V* value for configuration A-5 is higher in flat-roofed buildings than in pitched-roofed buildings. This difference is attributed to the higher mean internal pressure in the flat-roof building compared to the pitched-roof for configuration A-5, causing the airstream to experience greater resistance and resulting in air accumulation inside the building.

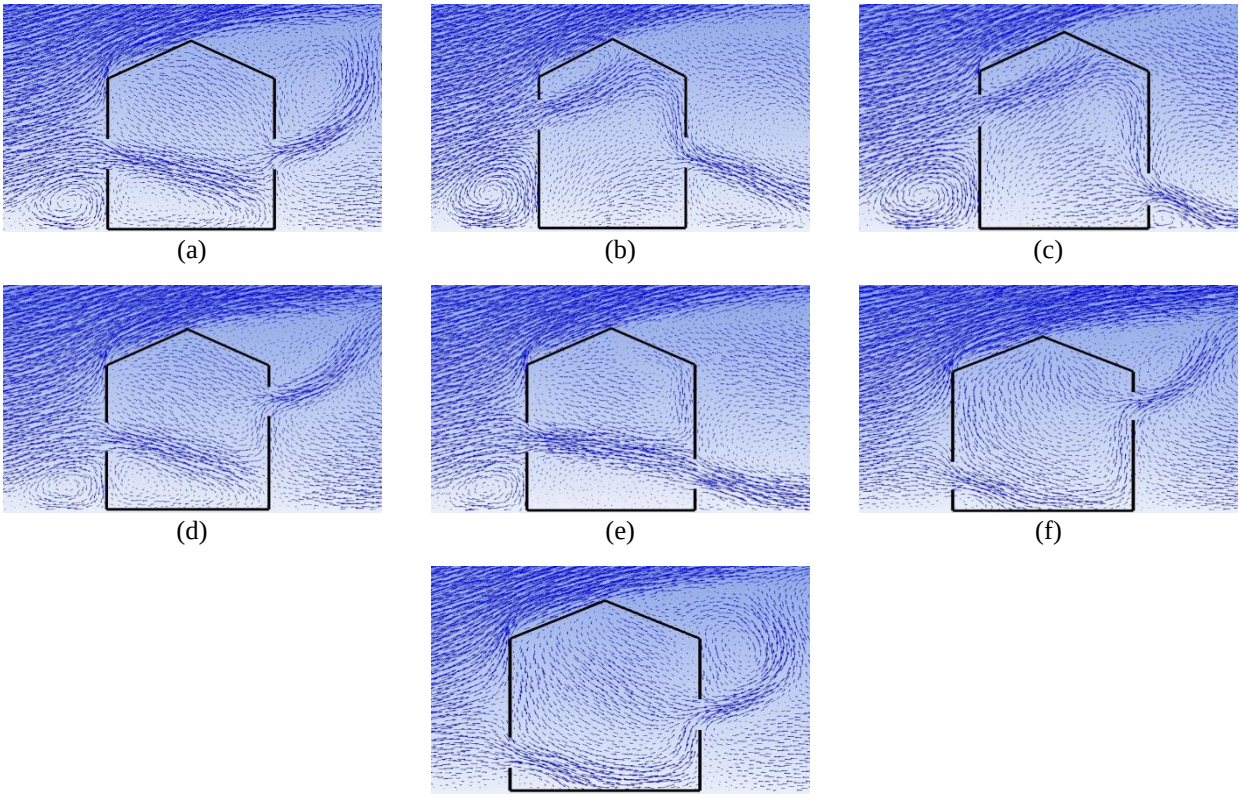

Figure 9. Velocity vector plot on the vertical mid-plane of pitched-roof building for configurations (a) S-0, (b) A-1, (c) A-2, (d) A-3, (e) A-4, (f) A-5, (g) A-6

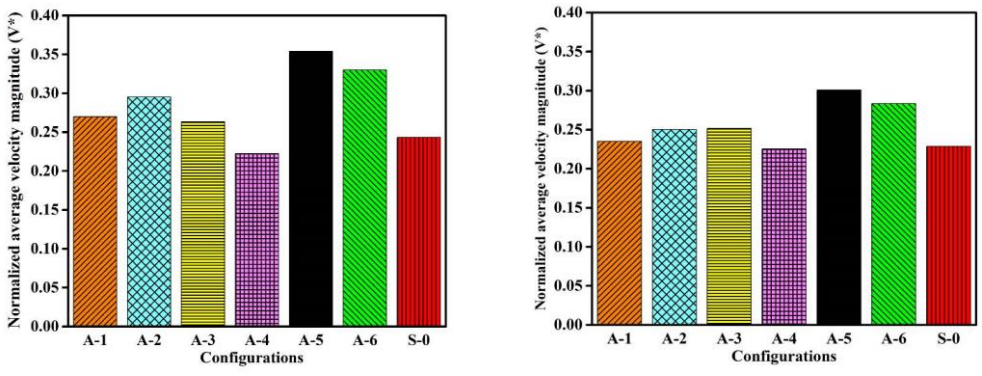

Figure 10. Normalised average velocity magnitude (V*) estimated for various configurations with (a) flat-roof and (b) pitched-roof building models

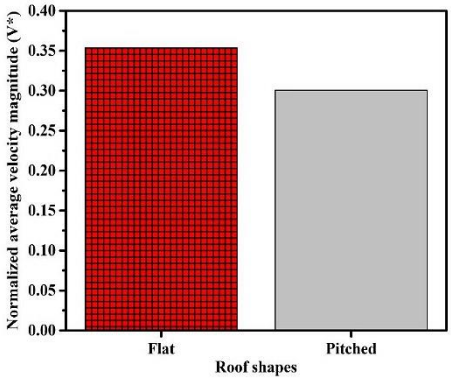

Figure 11. Comparison of normalised average velocity magnitude (V*) for configurations A-5 in flat and pitched-roof building models

3.3 Velocity Homogeneity Index (H)

The parameter velocity homogeneity index, *H*, is estimated using Eq. (8) as suggested by Cruz-Salas *et al.* [31]. H is also an indicator of IAD and is therefore related to IAQ. A higher value of H indicates enhanced IAQ.

$$H = 1 - \frac{\sigma_V}{V_{avg}} \tag{8}$$

where σ_V is the standard deviation of velocity magnitude in the occupying space, and V_{avg} is the average velocity magnitude.

The velocity homogeneity index (H), which measures the uniformity of airflow within a building, was evaluated for six asymmetric opening configurations and compared against the symmetric configuration (S-0) in a flat-roof building, as illustrated in Figure 12(a). The results indicate that the value of H is generally higher in asymmetric configurations than in the symmetric configuration, except for configuration A-4. Among all configurations, A-5 exhibited the peak H value, while A-4 had the lowest. Notably, H for configuration A-5 was observed to be 78.6% higher compared to S-0, demonstrating significant improvement in airflow mixing. Conversely, in A-4, the H value was 29.96% lower than that of S-0, suggesting reduced airflow uniformity. Additionally, while configurations A-1 and A-3 showed minor differences in H, configuration A-2 recorded a higher H value than both A-1 and A-3. Elevated H values in certain configurations suggest a more homogeneous distribution of air velocity throughout the building's interior. This reduces air stagnation, promotes better dilution of indoor contaminants, and hence improves overall air quality [32].

Furthermore, H values were analysed for pitched-roof buildings with identical configurations, and the comparison is presented in Figure 12(b). The variation in H for pitched-roofs followed a pattern similar to that observed in flat-roof buildings. For configuration A-5, the H value in pitched-roofs exceeded S-0 by 74.52%, slightly less than the corresponding increase observed in flat-roofs. In contrast, configuration A-4 showed a decrease of 28.85% in H compared to S-0. Interestingly, the pitched-roof results diverged from those of flat-roofs as configurations A-1 and A-2 had lower H values than A-3. Despite these variations, configuration A-5 consistently exhibited the highest H values across both building shapes, underscoring its efficiency in enhancing airflow uniformity. A detailed comparison of flat and pitched-roofs for configuration A-5, shown in Figure 13, revealed that H was higher in flat-roof buildings. This difference may be attributed to factors similar to those influencing variations in V*, as discussed in the study. These findings highlight the significant impact of roof shapes and opening configurations on airflow patterns, emphasizing the importance of optimal design for improved indoor air quality.

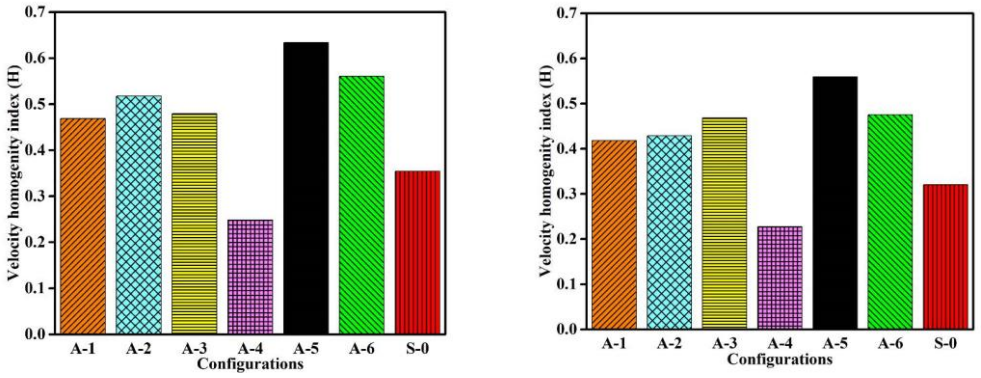

Figure 12. Velocity homogeneity index (H) calculated for various configurations with (a) flat-roof and (b) pitched-roof building models

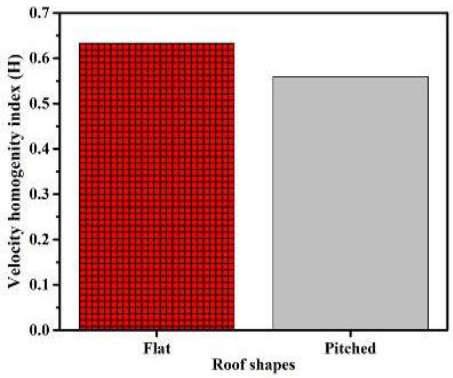

Figure 13. Comparison of normalised average velocity magnitude (H) for configurations A-5 in flat and pitched-roof building models

3.4 Air Change Rate (ACH)

The parameter air change rate (ACH) is also extensively used to measure the IAQ, as it is one of the practical methods of determining the IAQ [6]. The air change rate (ACH) can be determined mathematically by using Eq. (9). Here, ACH represents the number of times the fresh air is supplied to the indoor or ventilated space per hour. Therefore, higher ACH indicates improved IAQ.

$$ACH = \frac{60 \times Q}{Volume \text{ of the occupying space}} \tag{9}$$

here, Q represents the volume flow rate in m^3/min and the volume of the indoor space in m^3.

The calculated air change rates (ACH) for flat-roof and pitched-roof buildings with six different asymmetric opening configurations and one symmetric configuration are compared and shown in Figure 14. ACH in the symmetric configuration (S-0) is higher than the other asymmetric configurations, except A-4. The ACH attains the peak value for A-4, and the lowest ACH value is noted for the configuration A-5. Higher ACH means more recirculation of fresh air, which improves indoor air quality. The variation of ACH in A-1, A-2, and A-3 is less significant in both flat and pitched-roof buildings. Similar to flat-roof buildings, in pitched-roof buildings, too, the highest ACH is obtained for configuration A-4, and the lowest ACH is achieved for A-5. The ACH in A-4 is 6.65% higher than the symmetric configuration (S-0) in flat-roof buildings; however, in A-5, it is 26.65% lower than the S-0. Additionally, in pitched-roof buildings, ACH is higher in A-4 by 13.36% than S-0, and in A-5 it is 22.54% lower than S-0.

It is worth noting that the peak ACH value is obtained for configuration A-4 among all other configurations in both flat and pitched-roof building models. As discussed in the previous section, the formation of the continuous stream tube between the building's inlet and outlet in configuration A-4 causes an increase in airflow rate, resulting in a higher air change rate. However, the ACH is 2.8% higher in pitched-roof buildings compared to flat-roofs for configuration A-4 (Figure 15). This is because a more prominent recirculation region forms above the jet in the flat-roof model than in the pitched-roof, which weakens the stream tube in the flat-roof model and consequently lowers the ACH.

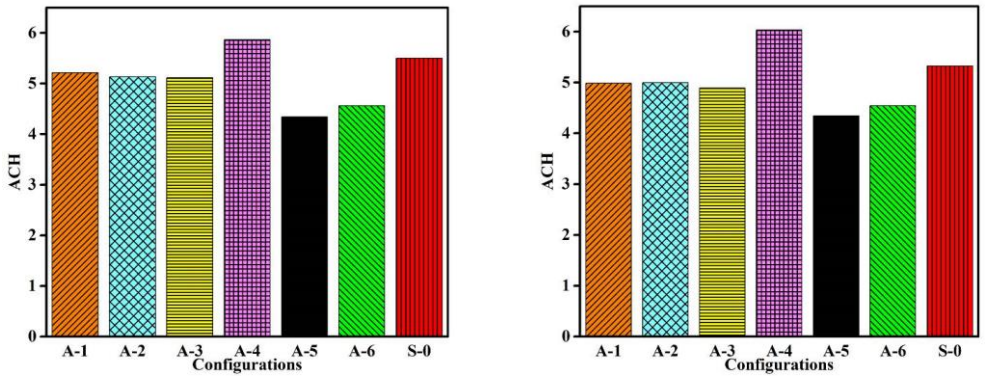

Figure 14. Comparison of air change rate (ACH) for various configurations in (a) flat-roof and (b) pitched-roof buildings

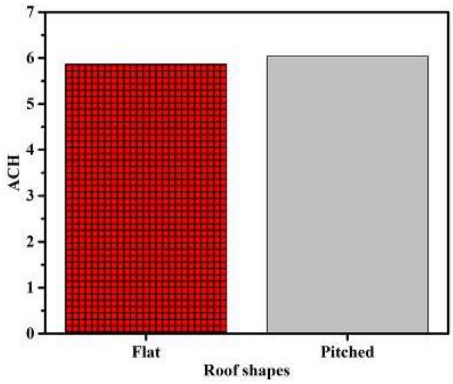

Figure 15. Comparison of ACH for configurations A-4 in flat and pitched-roof building models

4. CONCLUSIONS

This study investigates the effectiveness of natural ventilation in indoor spaces with two distinct building shapes: flat and pitched-roofs. Numerical simulations were conducted to analyse various configurations of openings, placed either axially or diagonally, to assess their impact on ventilation performance. The evaluation was based on three key parameters: normalised averaged velocity magnitude (V*), velocity homogeneity index (H), and air change rate (ACH). These parameters provide insights into indoor air distribution, mixing, and the rate of air replacement, which collectively determine the quality of natural ventilation. The results reveal that configurations with diagonally positioned openings generally yield better ventilation performance compared to axially positioned openings, irrespective of the roof shapes. Among all configurations tested, the flat-roofed building with the windward opening near the ground and the leeward opening near the roof (Configuration A-5) exhibited the highest values of V* and H. This indicates enhanced indoor air distribution and improved mixing due to the longer airflow path and increased turbulence, which effectively dilute indoor contaminants and improve air quality. Conversely, the highest ACH was observed in the pitched-roof building when the windward opening was positioned at mid-height and the leeward opening near the ground (Configuration A-4). This configuration facilitates a streamlined flow path with reduced resistance, enabling faster air exchange and more frequent replacement of indoor air with fresh outdoor air. These findings suggest that the optimal configuration for maximizing V* and H in flat-roofed buildings is A-5, whereas A-4 is the most effective for achieving high ACH in pitched-roof buildings. The study provides critical insights into optimizing natural ventilation performance through the strategic placement of openings in different building shapes. By identifying configurations that maximize ventilation efficiency, the findings can guide the design of sustainable building ventilation systems that reduce energy consumption while improving indoor air quality. These results are particularly relevant for architects and engineers aiming to design energy-efficient buildings that prioritize occupant health and comfort. Future research could explore the effects of varying opening shapes, the relative sizes of windward and leeward openings, and different incident wind directions on ventilation efficiency in both flat and pitched-roof buildings.

ACKNOWLEDGEMENTS

This study was not supported by any grants from funding bodies in the public, private, or not-for-profit sectors.

CONFLICT OF INTEREST

The authors declare that they have no conflict of interest.

AUTHORS' CONTRIBUTION

K. K. Das (Conceptualization; Methodology; Supervision)

R. Deka (Conceptualization; Formal analysis; Writing – original draft)

P. P. Borthakur (Formal analysis; Visualisation; Writing – review & editing)

C. J. Sarma (Formal analysis; Validation)

P. Singh (Resources; Methodology; Writing – review & editing)

AVAILABILITY OF DATA AND MATERIALS

The datasets generated and analysed during this study consist solely of numerical simulation results. All relevant data are included within this published article. Additional information is available from the corresponding author upon reasonable request.

ETHICS STATEMENT

This research did not involve human participants, animals, or sensitive data. Therefore, ethical approval and informed consent were not required.

REFERENCES

[1] Z. Yan, Y. Lan, "Modeling COVID-19 infection in a confined space," *Nonlinear Dynamics*, vol. 101, no. 3, pp. 1643–1651, 2020.

[2] K. Bilen, E. Urmamen, M. T. Topcu, I. Solmaz, "Evaluations on the energy identity certificate and the usability of calculation method of building energy performance (BEP)," *Sigma Journal of Engineering and Natural Science*, vol. 11, no. 1, pp. 103–113, 2020.

[3] Y. Jiang, D. Alexander, H. Jenkins, R. Arthur, Q. Chen, "Natural ventilation in buildings: Measurement in a wind tunnel and numerical simulation with large-eddy simulation," *Journal of Wind Engineering and Industrial Aerodynamics*, vol. 91, no. 3, pp. 331–353, 2003.

[4] C. Buratti, P. Domenico, "Mean age of air in naturally ventilated buildings: Experimental evaluation and CO_2 prediction by artificial neural networks," *Applied Sciences*, vol. 10, p. 1730, 2020.

[5] J. Zhou, Y. Hua, Y. Xiao, C. Ye, W. Yang, "Analysis of ventilation efficiency and effective ventilation flow rate for wind-driven single-sided ventilation buildings," *Aerosol and Air Quality Research*, vol. 21, no. 5, pp. 1–21, 2021.

[6] M. Bayoumi, "Improving indoor air quality in classrooms via wind-induced natural ventilation," *Modelling and Simulation in Engineering*, p. 1–14, 2021.

[7] H. Sacht, M. A. Lukiantchuki, "Window size and the performance of natural ventilation," *Procedia Engineering*, vol. 196, pp. 972–979, 2017.

[8] Y. Hou, C. Chen, Y. Zhou, Z. Yang, S. Wei, "Investigation of natural ventilation performance of large-space circular coal storage dome," *Building Simulation*, vol. 14, no. 4, pp. 1077–1093, 2021.

[9] N. F. M. Kasim, S. A. Zaki, M. S. M. Ali, N. Ikegaya, A. A. Razak, "Computational study on the influence of different opening positions on wind-induced natural ventilation in an urban cubical building array," *Procedia Engineering*, vol. 169, pp. 256–263, 2016.

[10] G. Y. Yoon, S. J. Lee, H. Kwon, J. J. Kim, "Effect of flow structures on natural ventilation performance in an office model," *Journal of Visualization*, vol. 26, no. 2, pp. 289–298, 2023.

[11] Y. Hwang, C. Gorlé, "Large-eddy simulations of wind-driven cross ventilation, part 2: Comparison of ventilation performance under different configurations," *Frontiers in Built Environment*, vol. 8, pp. 1–14, 2022.

[12] S. F. Díaz-Calderón, J. A. Castillo, G. Huelsz, "Evaluation of different window heights and façade porosities in naturally cross-ventilated buildings: CFD validation," *Journal of Wind Engineering and Industrial Aerodynamics*, vol. 232, p. 105263, 2023.

[13] S. Derakhshan, A. Shaker, "Numerical study of the cross-ventilation of an isolated building with different opening aspect ratios and locations for various wind directions," *International Journal of Ventilation*, vol. 16, no. 1, pp. 42–60, 2017.

[14] C. H. Hu, M. Ohba, R. Yoshie, "CFD modelling of unsteady cross-ventilation flows using LES," *Journal of Wind Engineering and Industrial Aerodynamics*, vol. 96, no. 10–11, pp. 1692–1706, 2008.

[15] T. Kobayashi, M. Sandberg, T. Fujita, E. Lim, N. Umemiya, "Numerical analysis of wind-induced natural ventilation for an isolated cubic room with two openings under small mean wind pressure difference," *Building and Environment*, vol. 226, p. 109694, 2022.

[16] H. Shetabivash, "Investigation of opening position and shape on natural cross ventilation," *Energy and Buildings*, vol. 93, pp. 1–15, 2015.

[17] Y. Tominaga, B. Blocken, "Wind tunnel analysis of flow and dispersion in cross-ventilated isolated buildings: Impact of opening positions," *Journal of Wind Engineering and Industrial Aerodynamics*, vol. 155, pp. 74–88, 2016.

[18] L. K. Moey, K. L. Chan, V. C. Tai, T. F. Go, P. L. Chong, "Investigation on the effect of opening position across an isolated building for wind-driven cross ventilation," *Journal of Mechanical Engineering and Sciences*, vol. 15, no. 2, pp. 8141–8152, 2021.

[19] P. Karava, T. Stathopoulos, A. K. Athienitis, "Airflow assessment in cross-ventilated buildings with operable façade elements," *Building and Environment*, vol. 46, no. 1, pp. 266–279, 2011.

[20] Y. Tominaga, S. Akabayashi, T. Kitahara, Y. Arinami, "Airflow around isolated gable-roof buildings with different roof pitches: Wind tunnel experiments and CFD simulations," *Building and Environment*, vol. 84, pp. 204–213, 2015.

[21] J. I. Perén, T. van Hooff, B. C. C. Leite, B. Blocken, "CFD analysis of cross-ventilation of a generic isolated building with asymmetric opening positions: Impact of roof angle and opening location," *Building and Environment*, vol. 85, pp. 263–276, 2015.

[22] F. Xing, D. Mohotti, K. Chauhan, "Experimental and numerical study on mean pressure distributions around an isolated gable-roof building with and without openings," *Building and Environment*, vol. 132, pp. 30–44, 2018.

[23] A. Hayati, M. Mattsson, M. Sandberg, "A wind tunnel study of wind-driven airing through open doors," *International Journal of Ventilation*, vol. 18, no. 2, pp. 113–135, 2018.

[24] J. Franke, A. Hellsten, H. Schlünzen, B. Carissimo, *Best Practice Guideline for the CFD Simulation of Flows in the Urban Environment*, COST Action 732, Hamburg, Germany, 2007, pp. C.1.1–C.1.11.

[25] Y. Tominaga, A. Mochida, R. Yoshie, H. Kataoka, T. Nozu, M. Yoshikawa, et al., "AIJ guidelines for practical applications of CFD to pedestrian wind environment around buildings," *Journal of Wind Engineering and Industrial Aerodynamics*, vol. 96, no. 10–11, pp. 1749–1761, 2008.

[26] B. Blocken, T. Stathopoulos, J. Carmeliet, "CFD simulation of the atmospheric boundary layer: Wall function problems," *Atmospheric Environment*, vol. 41, no. 2, pp. 238–252, 2007.

[27] D. Hargreaves, N. Wright, "The use of commercial CFD software to model the atmospheric boundary layer," in *The Fourth International Symposium on Computational Wind Engineering*, Yokohama, Japan, 2006, pp. 797–800.

[28] P. Karava, *Airflow Prediction in Buildings for Natural Ventilation Design*, Ph.D. dissertation, Concordia Univ., Montreal, QC, Canada, 2008.

[29] R. Ramponi, B. Blocken, "CFD simulation of cross-ventilation flow for different isolated building configurations: Validation with wind tunnel measurements and analysis of physical and numerical diffusion effects," *Journal of Wind Engineering and Industrial Aerodynamics*, vol. 104–106, pp. 408–418, 2012.

[30] P. Y. Cui, W. Q. Chen, J. Q. Wang, J. H. Zhang, Y. D. Huang, W. Q. Tao, "Numerical studies on issues of Reynolds-number independence for indoor airflow and pollutant dispersion within an isolated building," *Building Simulation*, vol. 15, no. 7, pp. 1259–1276, 2022.

[31] M. V. Cruz-Salas, J. A. Castillo, G. Huelsz, "Effect of wind-exchanger duct cross-section area and geometry on room airflow distribution," *Journal of Wind Engineering and Industrial Aerodynamics*, vol. 179, pp. 514–523, 2018.

[32] S. H. Park, K. R. Lee, S. J. Yook, H. B. Koo, "Enhancement and homogenization of indoor air quality in a classroom using a vertical airflow ventilation scheme," *Toxics*, vol. 10, no. 9, pp. 1–10, 2022.